ORNL/NUREG/TM-41

Quarterly Progress Report on the Zirconium Metal-Water Oxidation Kinetics Program Sponsored by the NRC Division of Reactor Safety Research for April–June 1976

J. V. Cathcart

OAK RIDGE NATIONAL LABORATORY
OPERATED BY UNION CARBIDE CORPORATION FOR THE ENERGY RESEARCH AND DEVELOPMENT ADMINISTRATION

Printed in the United States of America. Available from
National Technical Information Service
U.S. Department of Commerce
5285 Port Royal Road, Springfield, Virginia 22161
Price: Printed Copy $~~4.50~~ $4.00, Microfiche $2.25

ORNL/NUREG/TM-41
NRC-3

Contract No. W-7405-eng-26

METALS AND CERAMICS DIVISION

QUARTERLY PROGRESS REPORT ON THE ZIRCONIUM METAL–WATER OXIDATION KINETICS PROGRAM SPONSORED BY THE NRC DIVISION OF REACTOR SAFETY RESEARCH FOR APRIL–JUNE 1976

J. V. Cathcart

AUGUST 1976

Manuscript Completed - July 20, 1976

Date Published

Work performed by Union Carbide Corporation for the U.S. Regulatory Commission under Agreements 40-551-75 and 40-552-75.

OAK RIDGE NATIONAL LABORATORY
Oak Ridge, Tennessee 37830
operated by
UNION CARBIDE CORPORATION
for the
ENERGY RESEARCH AND DEVELOPMENT ADMINISTRATION

CONTENTS

SUMMARY

Except for scoping tests of the influence of steam pressure on the oxidation behavior of Zircaloy-4, the experimental phase of the reaction rate studies was completed. Kinetic data for the isothermal steam-Zircaloy reaction between 900 and 1500°C (1652—2732°F) are reported, and the parabolic rate constants for the growth of oxide, alpha, and Xi (oxide + alpha) layers as well as that for total oxygen consumption are given in the form of Arrhenius equations. The transient temperature oxidation experiments are described along with scoping tests of the effects of steam impurities and small variations in alloy content. A study of the oxidation of Zircaloy in high pressure steam was initiated, and a final report on our investigation of the diffusion of oxygen in β-Zircaloy-4 was prepared. The results of a limited number of oxygen diffusivity measurements in oxygen-stabilized α-Zircaloy-4 are also reported.

ZIRCONIUM METAL–WATER OXIDATION KINETICS

J. V. Cathcart

Metals and Ceramics Division

INTRODUCTION

The objective of this program is to provide a basic data set on which more reliable predictions of the transient temperature oxidation behavior of Zircaloy-4 in steam may be based. Major tasks involve 1) the determination of the isothermal rates of oxidation of Zircaloy between 900 and 1500°C (1652–2732°F); 2) the measurement of diffusivity of oxygen in β-Zircaloy-4 in the same temperature range; and 3) the development of a suitable computer code to predict oxidation behavior under transient temperature conditions.

During the past quarter a final report on the diffusion work was prepared. Except for the scoping tests of the effect of steam pressure on the isothermal rate of oxidation of Zircaloy, the experimental phase of the reaction rate studies was completed, and correlations for the parabolic rate constants as a function of temperature were established for oxide, alpha, and Xi (oxide + alpha) layer growth and for total oxygen consumption. The construction of the high pressure steam oxidation apparatus was begun, and progress on the verification of our computer code continued.

REACTION RATE STUDIES

R. E. Pawel, R. A. McKee, R. E. Druschel, J. J. Campbell,
E. T. Rose, and S. H. Jury*

Measurements of the oxide and alpha layer thicknesses have now been made for the complete basic set of isothermal steam oxidation experiments

---

*Consultant from Chemical Engineering Dept., Univ. of Tennessee, Knoxville, Tennessee.

conducted in the MiniZWOK apparatus. Parabolic growth behavior for both phases was observed for reactions at temperature above 1000°C (1832°F), while departures from parabolic kinetics were observed for the oxide phase at temperatures below 1000°C (1832°F). The data were analyzed in terms of parabolic growth kinetics, and rate constants were determined for the kinetic parameters for (1) oxide layer growth, (2) alpha layer growth, (3) Xi layer (oxide + alpha) growth, and (4) total oxygen consumed. The temperature dependence of these rate constants could be represented accurately by simple Arrhenius expressions. A statistical treatment of the data is in progress.

A number of transient-temperature steam oxidation tests were completed this quarter. In addition, a series of scoping tests in which small additions of nitrogen, oxygen, and hydrogen were made to the steam was also completed. These specimens are presently being examined.

The kinetic data for phase layer growth obtained during isothermal oxidation are being used to compute values of the diffusion coefficients in both the oxide and alpha phases of Zircaloy-4. These values, along with the directly measured diffusivities of oxygen in the beta phase, will be incorporated into the SIMTRAN program.

Isothermal Reaction Kinetics of Zircaloy-4

The kinetics of the reaction between the "standard" batch of Zircaloy-4 PWR fuel tubes* and steam were studied under essentially isothermal conditions over the temperature range 900–1500°C (1652–2732°F) at 50°C (90°F) intervals. The MiniZWOK oxidation apparatus was utilized to produce oxidized specimens that were then examined by metallographic

---

*Reactor grade Zircaloy-4 tubing from Sandvik Special Metals Corp., Spec. No. ASTM B353-71/MRBT-1, with exceptions; Cert. No. 75153; Lot No. 7FD 11. OD: 1.0922 cm; Wall THK; .0635 cm. Nominal Composition, (wt %); 1.60% Sn, .25% Fe, .12% Cr, .12% O, .009% C, .003% N, .0025% H.

methods in order to obtain the basic kinetic parameters. For each temperature investigated, at least ten specimens were oxidized; the oxidation times at each temperature were chosen to enable an accurate description of the kinetics to be obtained, yet to avoid problems that arise at longer oxidation times where excessive oxygen solution in the beta phase occurs.

Many of the experimental procedures used in the data gathering process have been discussed in detail in previous quarterly reports. Thus, we will include here only a cursory description of the procedures except where certain points have not previously received attention.

Experimental

A schematic diagram of the MiniZWOK steam-oxidation apparatus is shown in Fig. 1. This apparatus has been improved in a number of ways since its inception and has performed efficiently in producing well-characterized experiments for the rather extreme experimental conditions that were necessary. An experiment in MiniZWOK may be described briefly as follows: A 3 cm length of PWR tubing was instrumented at its mid-point on the inner surface with three Pt vs Pt—10% Rh thermocouples spot-welded to the Zircaloy via tantalum tabs. Two (diametrically opposed) thermocouples were connected to the Computer-Operated-Data-Acquisition System, CODAS-III, which recorded an accurate time-temperature history for these points on each specimen. The third thermocouple was connected to the furnace controller-recorder system, which drove the specimen through the desired time-temperature cycle by means of the quad-elliptical radiant heating furnace surrounding the specimen.

The instrumented specimen was mounted on an appropriately machined quartz support tube, as shown in the figure, and positioned in a larger quartz tube which served as the reaction chamber. During an experiment, steam flowed from a boiler through the annulus past the outer surface of the specimen. A slight positive pressure of helium was maintained on the inner assembly to prevent leakage of steam into the interior of

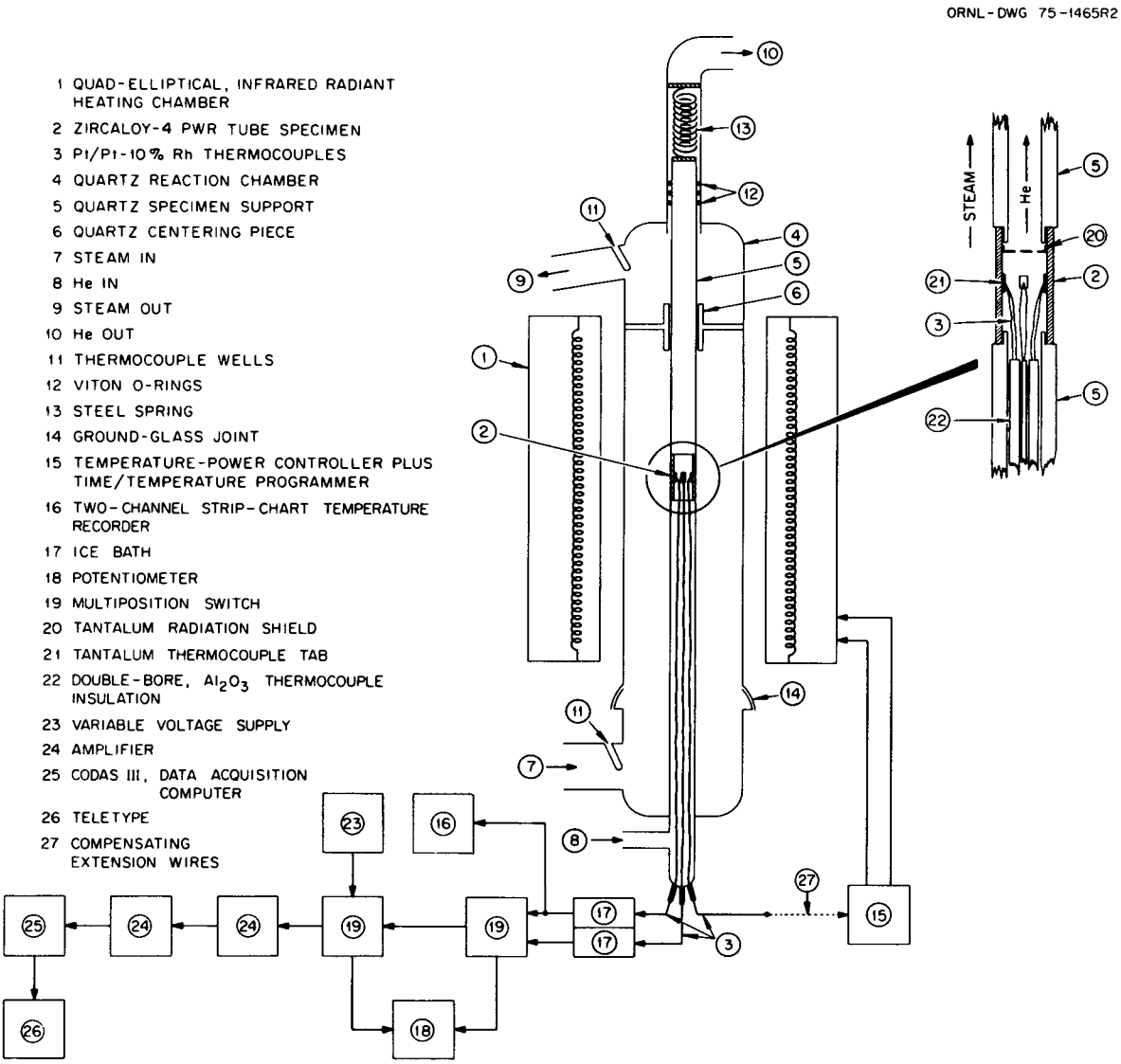

Fig. 1. Schematic diagram of MiniZWOK Oxidation Apparatus.

of the tube. This configuration was thought to be a most efficient one for minimizing thermocouple errors due to thermal and electrical shunting. An evaluation of the thermometry techniques associated with this apparatus led to the conclusion that the probable errors in temperature measurements were within ±4°C (7.2°F) at 900°C (1652°F) and within ±6°C (10.8°F) at 1500°C (2732°F).[1]

We have shown previously several typical time-temperature recorder traces from MiniZWOK experiments that illustrate the excellent response of both furnace and controller. Programmed heating rates greater than 100°C/s (180°F/s) were used routinely without difficulty in this unit.

Measurements

After each steam-oxidation experiment was completed, the specimen was removed from the apparatus, sectioned on a diamond-impregnated wheel, mounted in epoxy, polished, and prepared for metallographic examination by the etch-anodization treatment previously described.[2] Care was taken to insure that the final polished section was at the elevation which included the weld positions of all three thermocouple installations. Thus, the phase thickness measurements could be made in very close proximity to the monitor thermocouple locations. In the light of the general observation that the temperature (and thus the product layer thicknesses) of the specimens oxidizing in MiniZWOK exhibited a circumferential variation, it was important to associate each phase thickness measurement position with a point on the specimen having a known time-temperature history.

The two monitor thermocouple stations on each specimen were always located in the same relative position with respect to the heating lamps within the furnace. These positions were generally the "hot" positions, and, thus, the extent of the temperature variation around a specimen could only be determined by rotating the specimen (or furnace) during oxidation or inferred by measuring the circumferential variation in product layer thicknesses after the experiment. At low temperatures, these variations

were small. A plot of oxide and alpha layer thicknesses after oxidation at 1153°C (2107°F) as a function of angular position on the circumference of the specimens is presented in Fig. 2. While the periodicity is evident, the magnitude of the variation is seen in this case to be little more than the normal data scatter. At higher temperatures, the effect was generally more pronounced. Figure 3 illustrates the variation observed after an experiment at 1504°C (2739°F). Although in this case, the temperature-time cycles recorded by the two monitor thermocouples located at approximately 0 and 180 degrees were virtually the same, the thickness variations observed over the whole specimen imply that a maximum temperature variation of about ±15°C (27°F) existed. The periodicity of the temperature variation is consistent with the furnace geometry, and "cold" positions corresponding to the location of the two furnace seams. A case where the two monitor

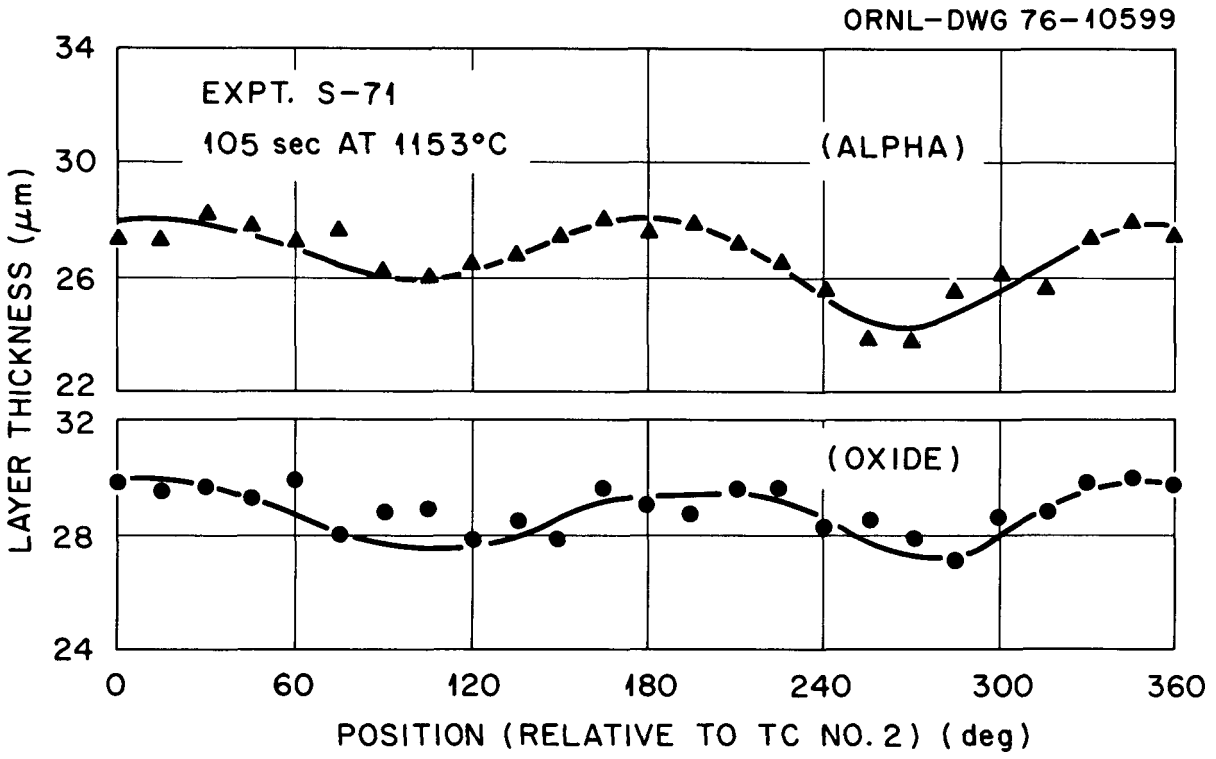

Fig. 2. Variation in oxide and alpha thicknesses on Specimen S-71, oxidized nominally 105 s at 1153°C (2107°F). Thermocouple No. 2 located at approx 0°; thermocouple No. 3 at approx 180°.

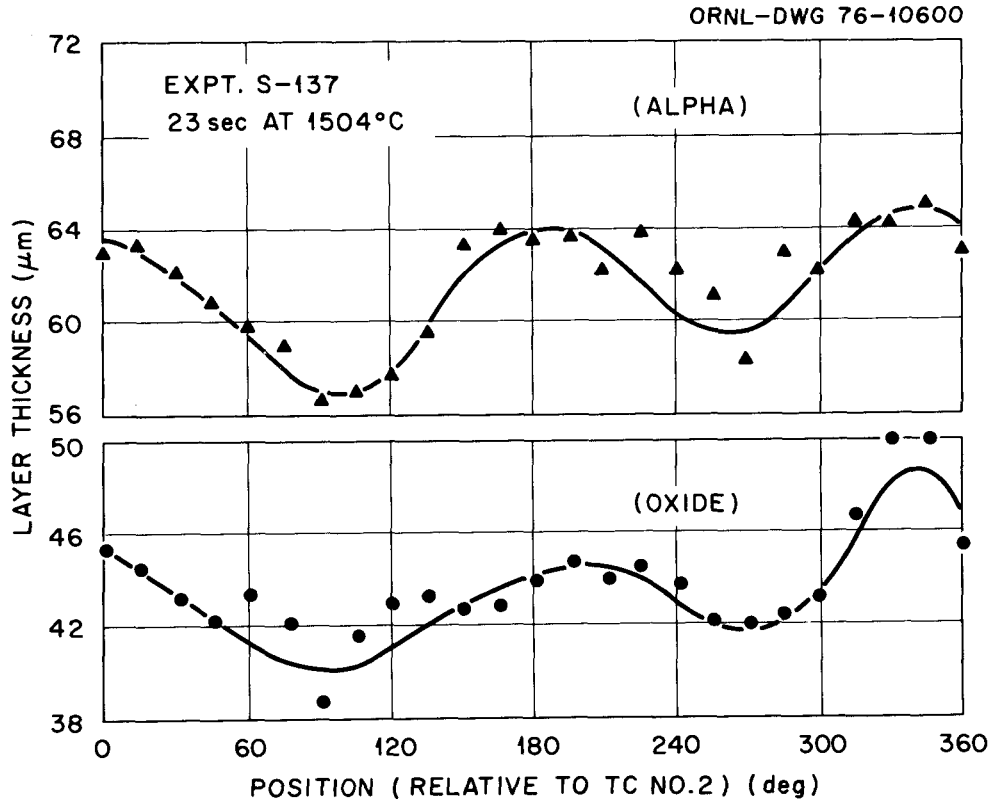

Fig. 3. Variation in oxide and alpha thicknesses on Specimen S-137, oxidized nominally 22 s at 1504°C (2739°F). Thermocouple No. 2 located at approx 0°; Thermocouple No. 3 at approx 180°.

thermocouples registered different temperatures is shown in Fig. 4. Here, the measured temperature difference accounted accurately for the measured phase thickness difference. The maximum variation in layer thicknesses over the whole specimen can be accounted for by a temperature variation of about ±20°C (36°F).

The existence of circumferential variations in temperature about a specimen made it mandatory that a high degree of correspondence exist between the points of temperature and layer thickness measurements. Thus, layer thicknesses were measured to coincide with each of the monitor thermocouple positions. In order to reduce errors in the thickness measurements due to artifacts and other sources, the average of seven measurements made at 5° intervals ±15° from each thermocouple position was used.

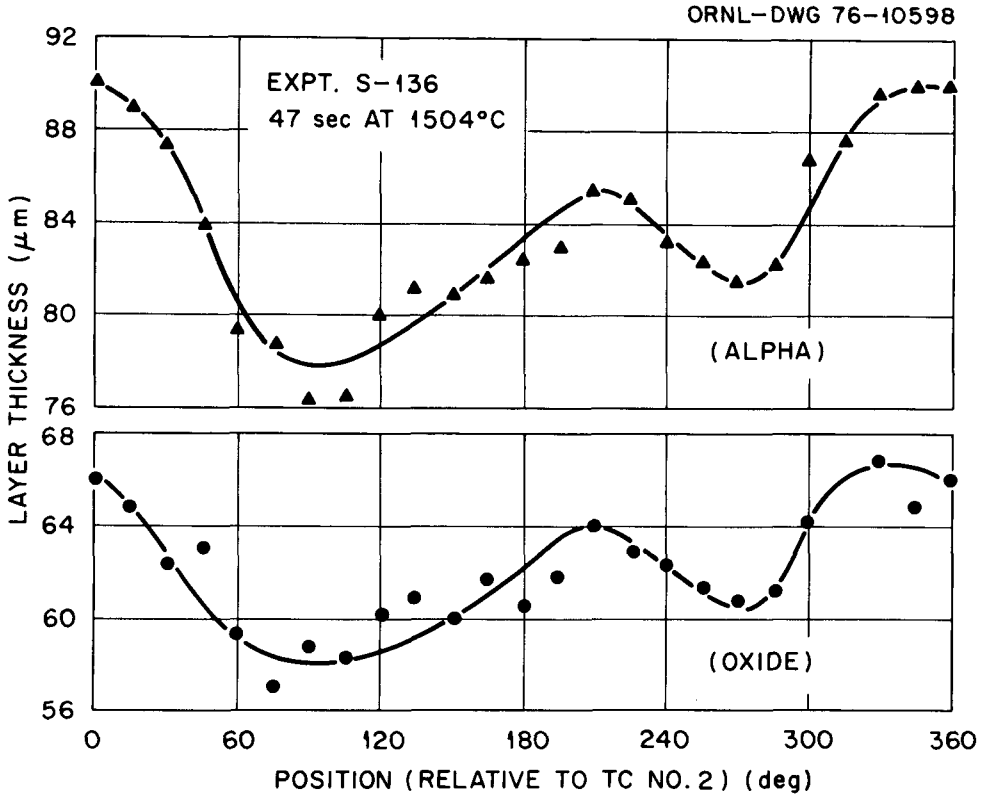

Fig. 4. Variations in oxide and alpha thicknesses on Specimen S-136, oxidized nominally 47 s at 1504°C (2739°F). Thermocouple No. 2 located at approx 0°; Thermocouple No. 3 at approx 180°.

The normalization of the individual time-temperature excursions for a set of experiments to equivalent isothermal excursions at some assigned, average, temperature represents an important part of the kinetic data treatment where a multispecimen technique is used. This procedure has been discussed previously.[2,3] Basically (for a thermally activated process) if the actual temperature $T_{(t)}$ is known as a function of time, t, then the equivalent time, $t_{(eff)}$, for reaction under isothermal conditions at an assigned temperature $T_{(eff)}$ is given by

$$t_{(eff)} = \frac{\int_0^t \exp\left[-Q/RT_{(t)}\right] dt}{\exp\left[-Q/RT_{(eff)}\right]} \qquad (1)$$

where

R = gas constant, 1.987 cal/g mol − °K,

Q = activation energy for the process under consideration, cal/g mol.

For each set of experiments conducted in the MiniZWOK apparatus, an "average" temperature of the set was chosen, and the equivalent time at that temperature was calculated according to Eq. (1) for each experiment. In these calculations, an activation energy of 40 Kcal/mol was assumed to apply for each rate process. However, sensitivity tests showed that the time corrections to most experiments varied only slightly for values of Q in the range of 30 to 50 Kcal/mol. Moreover, as part of an iterative calculation check, rate constants were computed for oxide and alpha layer growth at 1253 and 1504°C using the actual Q values for each. The average change in the rate constant observed using the iterative method for computation of the times was less than 0.5%; thus, we have concluded that Eq. (1) performs accurate normalizations on the MiniZWOK excursions using a mean value for the activation energy. Of course, the magnitude of the correction and its sensitivity to the precise values of the activation energy will depend upon the exact shape of the time-temperature cycle in relation to the desired isothermal.

The calculations of the effective oxidation times according to Eq. (1) were performed by computer. The CODAS system provided the basic time-temperature function, $T_{(t)}$, which, for the very-short-time experiments at the highest temperature, consisted of temperature readings on each thermocouple every 50 ms. For longer experiments the CODAS input to the program was appropriately modified with no appreciable loss in accuracy. It should be pointed out that where temperature differences existed between the monitor thermocouple positions during oxidation on a single specimen, the equivalent times associated with each position were generally different. The consistency of the experimental and calculated observations regarding this effect was regarded as further evidence of the accuracy of our temperature and layer-thickness measuring procedures.

Results

The procedures outlined above were used to obtain measurements of oxide layer thickness and alpha layer thickness as functions of time for each temperature investigated. In addition, the oxygen uptake for each specimen was calculated from the layer thickness measurements on the basis of a model that assumed that all the oxide was stoichiometric, that a linear oxygen concentration gradient existed in the alpha layer, and that a simple diffusion calculation would suffice for determining the amount of oxygen in the beta phase. These calculations may be refined in the future when a more precise Zircaloy-4/oxygen phase diagram becomes available. It should be noted, however, that several direct measurements of oxygen consumption (by weight gain), have agreed well with the values calculated on the above basis.[4]

The data obtained in this phase of our investigation are presented in Tables 1 to 13. At this stage of the analysis, we have discarded the results of experiments only when the experiment was obviously flawed. These were very few in number. The results of certain of the other experiments, also few in number, may be regarded statistically as "outliers" but have nevertheless still been included in the present data set. Additionally, for oxidation measurements at and above 1400°C (2552°F) instrumentation changes permitted complete and independent measurements of time and temperature at two positions on each specimen. For experiments below this temperature, only measurements at the No. 2 thermocouple position were considered in the analysis.

Correlation of the Data

An examination of the rates of growth of the oxide and alpha layers over the temperature range of this investigation revealed that parabolic growth kinetics applied to both phases at temperatures above 1000°C (1832°F) but only to the alpha phase below this temperature. The nonparabolic growth behavior of the oxide at ∿900°C (1652°F) was discussed in the last quarterly report.[3] The data set obtained at

Table 1. Steam Oxidation of Sandvik Zircaloy-4 PWR Tubing at 905°C (1661°F)

Expt. No.	Time (s)	Layer Thickness		Total Oxygen Consumed (mg/cm^2)
		oxide (μm)	alpha (μm)	
S-15	791.9	13.5	13.2	2.37
S-16	776.6	13.8	13.5	2.42
S-17	2088.7	17.4	18.2	3.08
S-18	1148.8	15.8	16.5	2.80
S-19	420.3	11.5	9.4	1.97
S-20	2088.7	17.7	18.3	3.13
S-21	1228.2	15.1	14.1	2.63
S-22	1509.5	17.0	20.4	3.08
S-23	1623.4	17.2	21.0	3.12
S-24	370.7	11.2	10.0	1.94

Table 2. Steam Oxidation of Sandvik Zircaloy-4 PWR Tubing at 956°C (1752.8°F)

Expt. No.	Time (s)	Layer Thickness		Total Oxygen Consumed (mg/cm^2)
		oxide (μm)	alpha (μm)	
S-49	1344.9	26.5	24.1	4.62
S-50	977.9	23.1	18.9	3.97
S-51	1595.7	26.2	25.2	4.61
S-52	690.6	21.3	15.7	3.62
S-53	774.6	22.5	16.9	3.83
S-54	1300.2	25.1	22.3	4.37
S-55	948.7	22.0	19.9	3.83
S-56	1634.5	26.3	26.4	4.65
S-57	412.2	17.9	13.0	3.04
S-58	428.7	18.0	15.3	3.11

Table 3. Steam Oxidation of Sandvik Zircaloy-4 PWR Tubing at 1001°C (1833.8°F)

Expt. No.	Time (s)	Layer Thickness		Total Oxygen Consumed (mg/cm^2)
		oxide (μm)	alpha (μm)	
S-37	1130.5	40.5	23.7	7.04
S-38	725.2	32.6	23.1	5.77
S-39	301.1	22.5	15.2	3.95
S-40	925.0	37.4	24.6	6.57
S-41	300.2	20.9	14.4	3.69
S-42	483.4	26.5	18.0	4.67
S-43	678.6	29.9	20.8	5.30
S-44	1104.1	38.6	26.1	6.81
S-45	915.5	34.5	24.6	6.13
S-46	475.7	25.9	17.6	4.57
S-47	493.4	27.1	19.5	4.80
S-48	299.4	21.3	13.8	3.73

Table 4. Steam Oxidation of Sandvik Zircaloy-4 PWR Tubing at 1050°C (1922°F)

Expt. No.	Time (s)	Layer Thickness		Total Oxygen Consumed (mg/cm^2)
		oxide (μm)	alpha (μm)	
S-59	576.4	40.7	32.7	7.50
S-61	518.6	38.6	24.3	6.93
S-62	663.5	43.1	35.6	7.98
S-63	351.4	32.1	27.7	5.97
S-64	482.7	37.4	27.6	6.83
S-65	338.6	30.9	24.5	5.69
S-66	833.2	48.4	36.0	8.85
S-67	763.0	44.7	35.7	8.26
S-68	204.7	24.2	23.4	4.57
S-69	209.0	24.6	23.4	4.63

Table 5. Steam Oxidation of Sandvik Zircaloy-4 PWR Tubing at 1101°C (2013.8°F)

Expt. No.	Time (s)	Layer Thickness		Total Oxygen Consumed (mg/cm^2)
		oxide (μm)	alpha (μm)	
S-25	495.6	45.7	41.6	8.77
S-26	252.7	33.5	33.0	6.49
S-27	313.4	36.6	36.6	7.12
S-28	512.4	47.1	45.4	9.10
S-29	348.1	37.2	37.0	7.25
S-30	383.4	40.8	37.1	7.82
S-31	252.1	33.3	24.5	6.22
S-32	159.5	26.0	23.1	4.97
S-33	173.9	29.4	26.9	5.61
S-35	449.3	45.7	43.5	8.79
S-36	458.9	44.6	44.5	8.66

Table 6. Steam Oxidation of Sandvik Zircaloy-4 PWR Tubing at 1153°C (2107.4°F)

Expt. No.	Time (s)	Layer Thickness		Total Oxygen Consumed (mg/cm^2)
		oxide (μm)	alpha (μm)	
S-70	269.5	43.0	40.6	8.42
S-71	104.8	28.9	27.9	5.64
S-72	343.3	50.2	47.7	9.82
S-73	193.7	37.6	38.0	7.42
S-74	339.0	48.9	46.7	9.59
S-76	249.4	42.4	42.6	8.36
S-77	108.6	29.1	29.5	5.73
S-78	169.9	37.0	37.4	7.27
S-79	388.2	53.2	46.5	10.29
S-80	29.6	16.8	15.8	3.24
S-81	29.9	16.9	15.9	3.26

Table 7. Steam Oxidation of Sandvik Zircaloy-4 PWR Tubing at 1203°C (2197.4°F)

Expt. No.	Time (s)	Layer Thickness		Total Oxygen Consumed (mg/cm^2)
		oxide (μm)	alpha (μm)	
S-82	236.4	49.4	53.5	10.03
S-83	160.2	42.8	44.7	8.59
S-84	126.6	38.9	41.0	7.81
S-85	280.2	53.5	54.9	10.78
S-86	234.6	50.2	51.6	10.09
S-88	56.1	26.6	28.2	5.33
S-89	171.8	43.2	44.0	8.66
S-90	66.1	28.6	30.9	5.75
S-91	111.2	37.2	39.7	7.46

Table 8. Steam Oxidation of Sandvik Zircaloy-4 PWR Tubing at 1253°C (2287.4°F)

Expt. No.	Time (s)	Layer Thickness		Total Oxygen Consumed (mg/cm^2)
		oxide (μm)	alpha (μm)	
S-92	240.3	59.2	67.2	12.30
S-93	189.0	54.2	61.3	11.21
S-95	50.7	30.2	34.2	6.20
S-97	90.2	39.5	44.3	8.12
S-98	62.5	32.3	37.7	6.69
S-99	117.8	43.5	50.2	9.02
S-100	55.5	30.3	36.4	6.31
S-101	169.3	50.7	60.2	10.59
S-102	226.4	58.5	66.9	12.15
S-103	48.6	30.0	34.3	6.16

Table 9. Steam Oxidation of Sandvik Zircaloy-4 PWR Tubing at 1304°C (2379.2°F)

Expt. No.	Time (s)	Layer Thickness oxide (μm)	Layer Thickness alpha (μm)	Total Oxygen Consumed (mg/cm^2)
S-1	138.4	56.2	66.9	11.87
S-3	151.4	59.7	71.8	12.61
S-4	83.4	44.9	53.4	9.45
S-5	124.4	51.7	61.7	10.96
S-6	123.2	53.1	60.6	11.13
S-7	32.9	28.9	32.5	6.01
S-8	30.0	27.9	31.7	5.81
S-9	111.1	50.1	58.9	10.57
S-10	62.2	38.2	45.2	8.05
S-11	79.9	41.2	48.6	8.72
S-12	59.3	36.4	42.8	7.68
S-13	57.7	36.5	42.2	7.67
S-14	34.3	28.0	32.4	5.89

Table 10. Steam Oxidation of Sandvik Zircaloy-4 PWR Tubing at 1352°C (2465.6°F)

Expt. No.	Time (s)	Layer Thickness oxide (μm)	Layer Thickness alpha (μm)	Total Oxygen Consumed (mg/cm^2)
S-104	112.8	62.3	78.1	13.36
S-105	80.8	52.7	66.9	11.33
S-106	69.5	46.9	60.5	10.16
S-107	73.1	49.8	63.2	10.71
S-108	28.3	31.8	41.3	6.85
S-109	90.1	53.7	70.3	11.66
S-110	32.4	32.5	39.6	6.96
S-111	50.9	40.6	52.1	8.78
S-112	116.5	60.9	79.3	13.21

Table 11. Steam Oxidation of Sandvik Zircaloy-4 PWR Tubing at 1404°C (2559.2°F)

Expt. No.	Time (s)	Layer Thickness		Total Oxygen Consumed (mg/cm^2)
		oxide (μm)	alpha (μm)	
S-114-TC-2	72.7	58.4	78.3	12.84
S-114-TC-3	62.2	53.4	70.9	11.74
S-115-TC-2	29.7	38.7	51.0	8.45
S-115-TC-3	28.6	35.2	49.2	7.84
S-116-TC-2	45.7	45.7	62.9	10.12
S-116-TC-3	42.6	44.7	60.4	9.85
S-117-TC-2	14.3	28.0	36.8	6.08
S-117-TC-3	13.5	26.1	35.7	5.74
S-118-TC-2	11.2	24.5	31.8	5.31
S-118-TC-3	10.4	23.4	30.7	5.09
S-119-TC-2	56.4	51.6	67.5	11.29
S-119-TC-3	54.2	48.8	65.7	10.79
S-120-TC-2	44.8	47.1	62.2	10.29
S-120-TC-3	43.4	45.1	60.4	9.92
S-121-TC-2	27.5	39.1	51.1	8.47
S-121-TC-3	29.8	39.2	51.4	8.53
S-122-TC-2	74.1	59.0	77.3	12.92
S-122-TC-3	78.9	60.3	77.6	13.18
S-123-TC-2	29.3	39.0	50.4	8.46
S-123-TC-3	26.5	35.1	47.2	7.73

Table 12. Steam Oxidation of Sandvik Zircaloy-4 PWR Tubing at 1454°C (2649.2°F)

Expt. No.	Time (s)	Layer Thickness		Total Oxygen Consumed (mg/cm^2)
		oxide (μm)	alpha (μm)	
S-124-TC-2	57.1	61.8	81.4	13.64
S-124-TC-3	54.0	59.7	79.1	13.20
S-125-TC-2	25.1	41.5	56.5	9.20
S-125-TC-3	23.2	40.7	53.4	8.94
S-126-TC-2	27.9	45.5	59.4	9.96
S-126-TC-3	26.1	42.2	57.4	9.36
S-127-TC-3	53.3	58.7	78.0	13.01
S-128-TC-2	27.3	42.8	58.7	9.52
S-128-TC-3	26.4	42.5	57.4	9.41
S-129-TC-2	13.7	32.6	42.4	7.11
S-129-TC-3	14.9	32.6	42.0	7.14
S-130-TC-2	43.5	54.5	72.6	12.04
S-130-TC-3	43.1	54.6	72.2	12.03
S-131-TC-2	47.2	56.4	74.3	12.44
S-131-TC-3	42.0	52.6	68.9	11.61
S-132-TC-2	15.3	32.3	41.8	7.10
S-132-TC-3	14.5	31.0	40.6	6.84
S-133-TC-2	36.8	49.7	64.9	10.95
S-133-TC-3	34.5	47.5	62.9	10.51

Table 13. Steam Oxidation of Sandvik Zircaloy-4 PWR Tubing at 1504°C (2739.2°F)

Expt. No.	Time (s)	Layer Thickness		Total Oxygen Consumed (mg/cm^2)
		oxide (μm)	alpha (μm)	
S-134-TC-2	31.8	53.6	72.1	11.98
S-134-TC-3	28.9	50.7	68.1	11.34
S-135-TC-2	33.0	57.8	75.7	12.76
S-135-TC-3	31.2	50.3	74.2	11.53
S-136-TC-2	47.0	65.6	88.2	14.65
S-136-TC-3	42.6	61.8	83.8	13.84
S-137-TC-2	22.8	45.8	63.6	10.29
S-137-TC-3	21.9	43.8	62.8	9.93
S-138-TC-2	7.6	27.3	38.7	6.13
S-138-TC-3	8.2	28.5	38.5	6.34
S-139-TC-2	53.2	73.7	97.6	16.29
S-141-TC-2	9.2	30.0	40.7	6.68
S-141-TC-3	8.9	28.9	40.8	6.50
S-142-TC-2	49.0	62.6	93.9	14.42
S-142-TC-3	50.0	62.5	91.4	14.34
S-143-TC-2	42.4	65.9	85.6	14.51
S-143-TC-3	37.8	57.5	80.3	12.97
S-150-TC-2	13.9	37.5	48.3	8.25
S-150-TC-3	13.2	35.5	48.6	7.93

956°C (1753°F) furnishes a good additional example of the different kinetic behavior exhibited by the oxide and alpha layers in this temperature range. These data are presented in Fig. 5. While the growth of the alpha layer appears to be accounted for satisfactorily by parabolic kinetics, departures from this behavior clearly exist for the oxide layer growth. In fact, the growth rate of the oxide layer at this temperature is more closely represented by a cubic rate expression. For this reason, parabolic rate constants will not be reported for oxide growth at temperatures below 1000°C (1832°F). Since the rate constants for Xi (oxide + alpha) layer growth and for total oxygen consumed involve the oxide growth parameter, they will also be subject to this limitation.

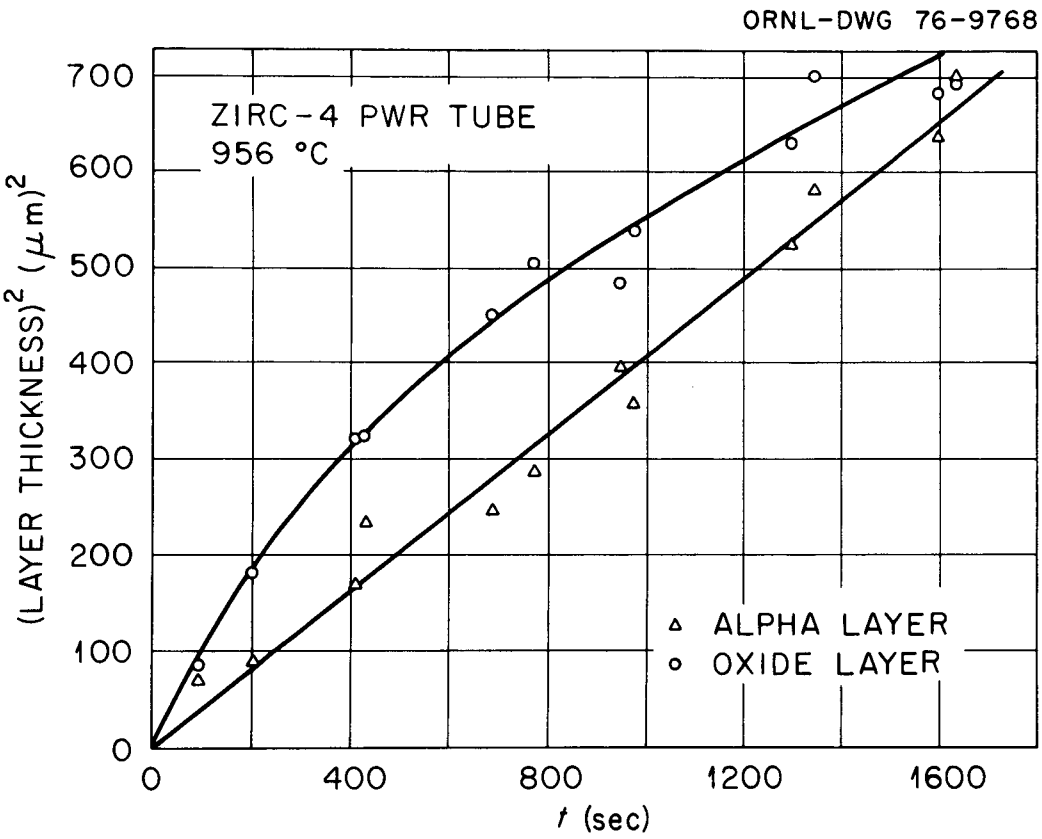

Fig. 5. Steam oxidation of Sandvik Zircaloy-4 PWR tubing in MiniZWOK apparatus at 956°C (1753°F). Example of nonparabolic growth in oxide layer.

The basic expression for the rate of a reaction where parabolic kinetics control is

$$\frac{dK}{dt} = \frac{1}{K}\frac{\delta_K^2}{2} \tag{2}$$

where

K is a kinetic parameter [i.e., oxide layer thickness, ϕ; alpha layer thickness, α; Xi (oxide + alpha) layer thickness, ξ; and total oxygen consumed, τ] and

$\frac{\delta_K^2}{2}$ is defined as the isothermal parabolic rate constant.*

The integrated form of this equation is

$$K^2 = K_o^2 + \delta_K^2 \, t \qquad (3)$$

and, thus, a plot of K^2 vs t should be linear with a slope of δ_K^2 and an intercept of K_o^2. Such plots of experimental data with nonzero values of K_o^2 might indicate deviations from strict parabolic behavior at short times, a pre-existing film or reaction layer on the specimen, or poor determinations of time-at-temperature for the reaction.

Parabolic rate constants for the four kinetic parameters ϕ, α, ξ, and τ were determined at each reaction temperature from the experimental data presented in Tables 1 through 13 by a least-squares treatment based on Eq. (3). Although we have used both approaches, the present rate constants were calculated on the basis that $K_o = 0$, which assumes "ideal" parabolic behavior. While the observed trend in the data was for K_o to have small, positive values, virtually no loss in statistical confidence was found as a result of this arbitrary assignment. In fact, the Arrhenius correlation of the rate constants calculated in this way exhibited a lower SSE (sum of squares of error), implying that this procedure gives a more consistent final result.

Illustrations of the kinetic behavior at the higher temperatures are given in Fig. 6 and 7. The data set obtained for oxidation at 1253°C (2287°F) includes measurements from only one reference point (the No. 2 thermocouple position). The data set for oxidation at 1454 (2649°F)

---

*It should be emphasized, see Eq. (2), that we express the parabolic rate constants as $\delta^2/2$. These values must be multiplied by two to give the slope of a plot of K^2 vs t [c.f., Eq. (3)]. Different authors use other conventions such as designating the parabolic rate constant as being the slope of a K^2 vs t plot. The matter comes down to the question of whether the factor of 1/2 obtained during the integration of KdK (i.e., $\int_o^K KdK = K^2/2$) in Eq. (2) is or is not incorporated in the rate constant.

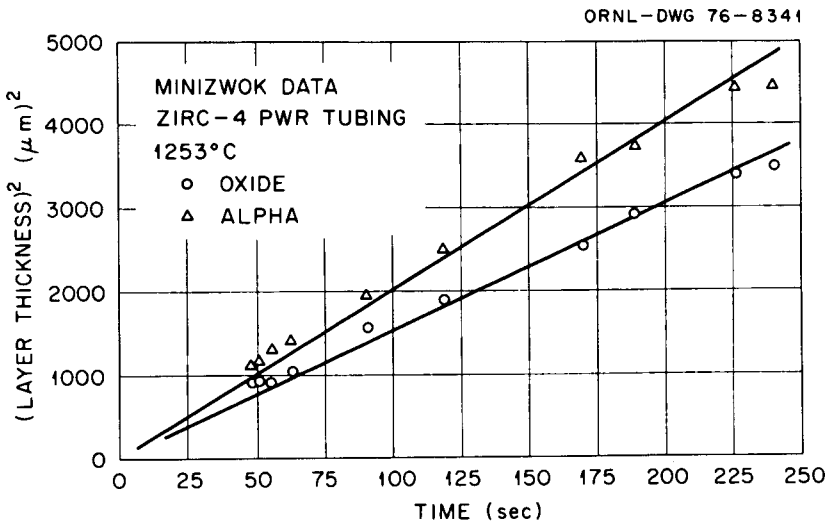

Fig. 6. Steam oxidation of Sandvik Zircaloy-4 PWR tubing in MiniZWOK apparatus at 1253°C (2287°F).

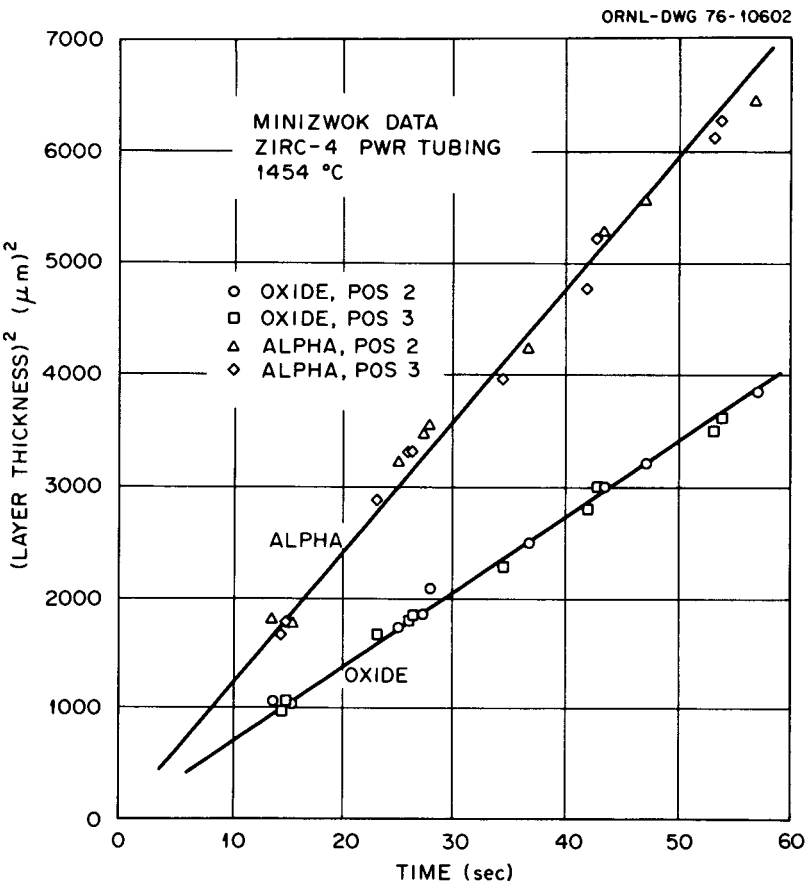

Fig. 7. Steam oxidation of Sandvik Zircaloy-4 PWR tubing in MiniZWOK apparatus at 1454°C (2649°F). Data from two monitor thermocouple positions for each specimen are plotted.

includes measurements from the two monitor thermocouple positions for each specimen, and the high degree of self-consistency of these measurements is evident. In each case, as in all cases for reaction above 1000°C (1832°F), the growth rates of these phases are well represented by parabolic growth kinetics, and the calculated parabolic rate constants have relatively narrow confidence intervals at the 90% level. The kinetics for Xi layer growth, ξ, and for total oxygen consumption, τ, behave similarly.

The parabolic rate constants from the present data sets are given in Table 14. It is interesting to observe that the scatter in the individual data, indicated by the statistical confidence in the rate constants, actually improved as the temperature increased. Part of the unexpected improvement must be associated with the fact that the measurements of interface positions are relatively more accurate at the higher temperatures because the system behaves more ideally.

Correlations of the rate constants in terms of simple Arrhenius relationships were, except for the alpha layer growth, restricted to the temperature range 1000—1500°C (1832—2732°F). In fact, because the rate constant for oxide growth at 1001°C (1834°F) appeared a little low compared to the rest of the data set, the least-squares and statistical representations were based on the data at and above 1050°C (1922°F). The four sets of parabolic rate constants are plotted in Arrhenius fashion in Figs. 8—11. The data are obviously well represented by this relationship, although a critical examination seems to indicate that some minor but systematic deviations exist. It should be mentioned, for example, that if the Arrhenius representation for the oxide and alpha rate constants are each linear with different slopes, then the corresponding representation for Xi *must* exhibit curvature. This effect appears negligible in the present case, and we have determined all of the expressions for the

Table 14. Parabolic Rate Constants for Isothermal Steam Oxidation of Sandvik Zircaloy-4 PWR Tubing

Temperature (°C)	Temperature (°F)	$\frac{\delta^2_\phi}{2}$ [Oxide] (cm^2/s) $\times 10^8$	Dev.[a] ± %	$\frac{\delta^2_\alpha}{2}$ [Alpha] (cm^2/s) $\times 10^8$	Dev.[a] ± %	$\frac{\delta^2_\xi}{2}$ [Xi] (cm^2/s) $\times 10^7$	Dev.[a] ± %	$\frac{\delta^2_\tau}{2}$ [Oxygen] $(g/cm^2)^2/s$ $\times 10^7$	Dev.[a] ± %
905	1661			0.1012	36.9				
956	1753			0.2027	12.4				
1001	1834	0.7072	8.0	0.3139	17.2	0.1961	8.7	0.2191	7.2
1050	1922	1.399	5.8	0.8493	28.2	0.4421	13.0	0.4725	6.0
1101	2014	2.171	8.0	1.950	21.2	0.8230	12.3	0.8066	7.6
1153	2017	3.631	4.9	3.254	13.7	1.375	8.3	1.387	5.0
1203	2197	5.389	10.4	5.872	14.1	2.251	11.9	2.185	9.7
1253	2287	7.663	6.7	10.07	8.2	3.530	7.2	3.300	6.0
1304	2379	11.41	4.8	15.93	6.3	5.431	5.2	5.078	4.2
1352	2466	16.51	6.9	27.10	4.4	8.592	4.6	7.693	5.2
1404	2559	23.51	4.1	41.22	4.4	12.70	3.9	11.31	3.4
1454	2649	33.66	3.5	59.01	4.1	18.18	3.6	16.41	3.0
1504	2739	45.25	8.7	85.95	3.4	25.58	4.5	22.79	6.0

[a] Maximum uncertainty at 90% confidence level.

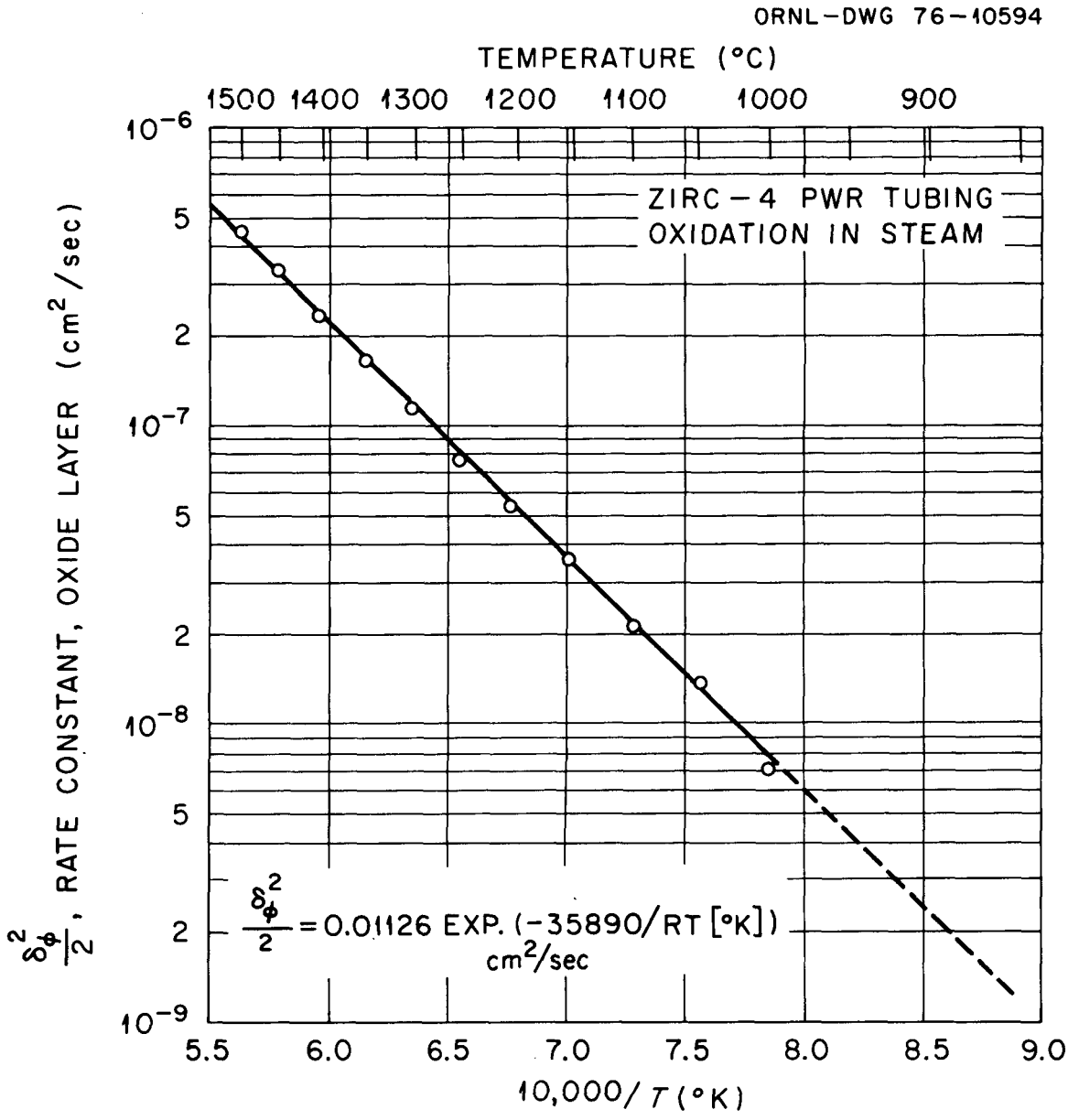

Fig. 8. Arrhenius plot of the parabolic rate constants for oxide layer growth from 1000 to 1500°C (1832–2732°F). Oxidation of Sandvik Zircaloy-4 PWR tubing in steam.

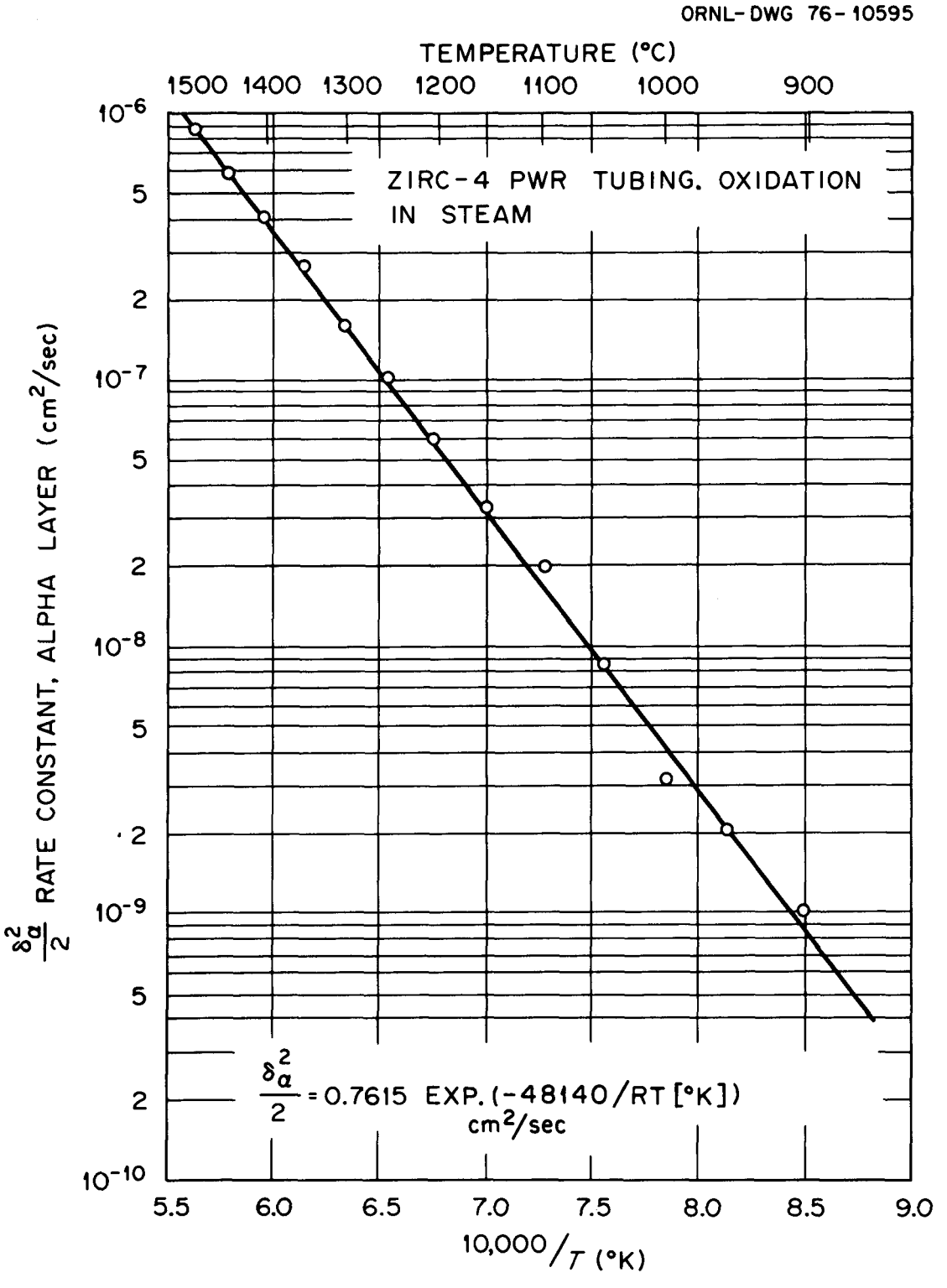

Fig. 9. Arrhenius plot of the parabolic rate constants for alpha layer growth from 900 to 1500°C (1652–2732°F). Oxidation of Sandvik Zircaloy-4 PWR tubing in steam.

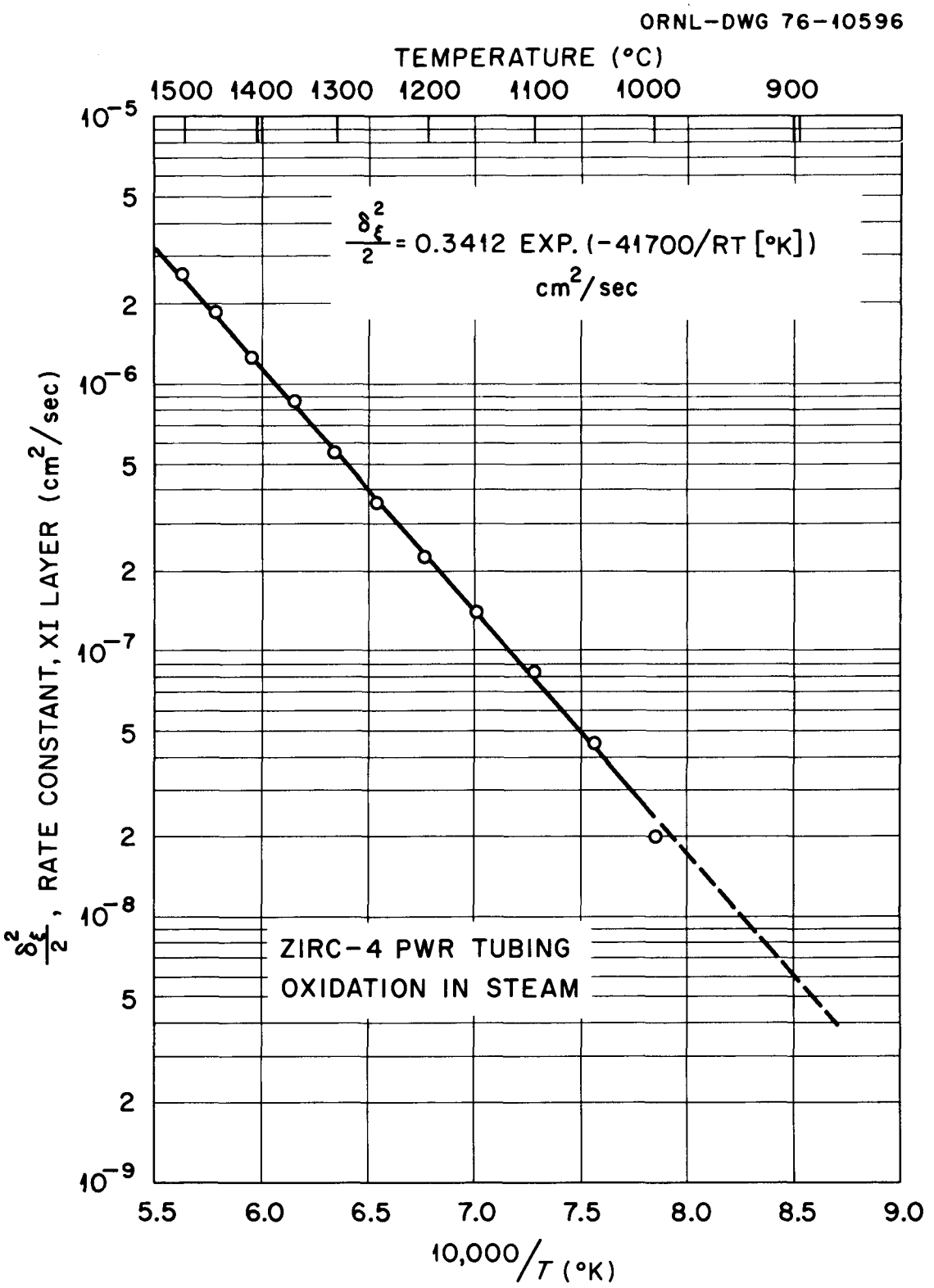

Fig. 10. Arrhenius plot of the parabolic rate constants for Xi (oxide + alpha) layer growth from 1000 to 1500°C (1832–2732°F). Oxidation of Sandvik Zircaloy-4 PWR tubing in steam.

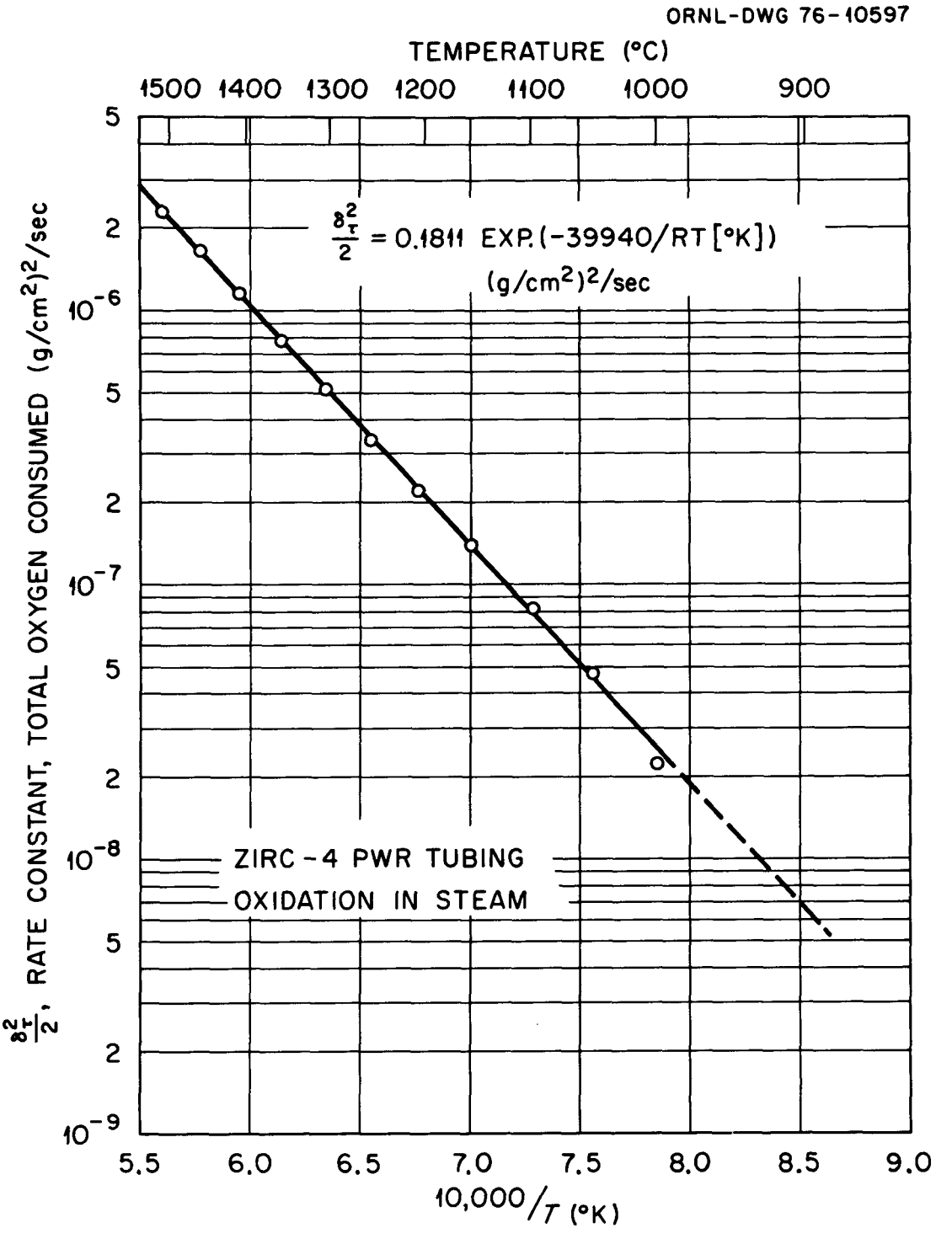

Fig. 11. Arrhenius plot of the parabolic rate constant for total oxygen consumption from 1000 to 1500°C (1832–2732°F). Oxidation of Sandvik Zircaloy-4 PWR tubing in steam.

temperature dependence of the parabolic rate constant on the basis of conformity to the Arrhenius equation. Thus:

$$\frac{\delta_{\phi}^2}{2} = .01126 \exp[-35890/RT(°K)] \text{ cm}^2/\text{s} . \quad (4)$$

$$\frac{\delta_{\alpha}^2}{2} = .7615 \exp[-48140/RT(°K)] \text{ cm}^2/\text{s} . \quad (5)$$

$$\frac{\delta_{\xi}^2}{2} = .3412 \exp[-41700/RT(°K)] \text{ cm}^2/\text{s} . \quad (6)$$

$$\frac{\delta_{\tau}^2}{2} = .1811 \exp[-39940/RT(°K)] (\text{g/cm}^2)^2/\text{s} . \quad (7)$$

where the subscripts ϕ, α, ξ, and τ refer to the kinetic parameters oxide layer thickness, alpha layer thickness, Xi layer thickness, and total oxygen consumed, respectively. The statistical treatments of these data are not yet complete, and will be reported at a later date.

Transient Temperature Oxidation Experiments

A variety of transient temperature oxidation experiments was performed in order to test the predictions of our computer code, SIMTRAN-I. The temperature-time profiles used are shown in Fig. 12. The very simple transients in Fig. 12a were designed to investigate the effects of variations in heating and cooling rates on code predictions. The profiles in Fig. 12b should reveal any effects related to changes in scale microstructure caused by an increase or decrease in temperature near the beginning or the end of the transient. Curve No. 1 in Fig. 12c simulates a transient calculated for a particular hypothetical LOCA; curve No. 2 is similar except that the maximum temperature of the blow-down peak was increased from 900°C (1652°F) to 1400°C (2552°F).

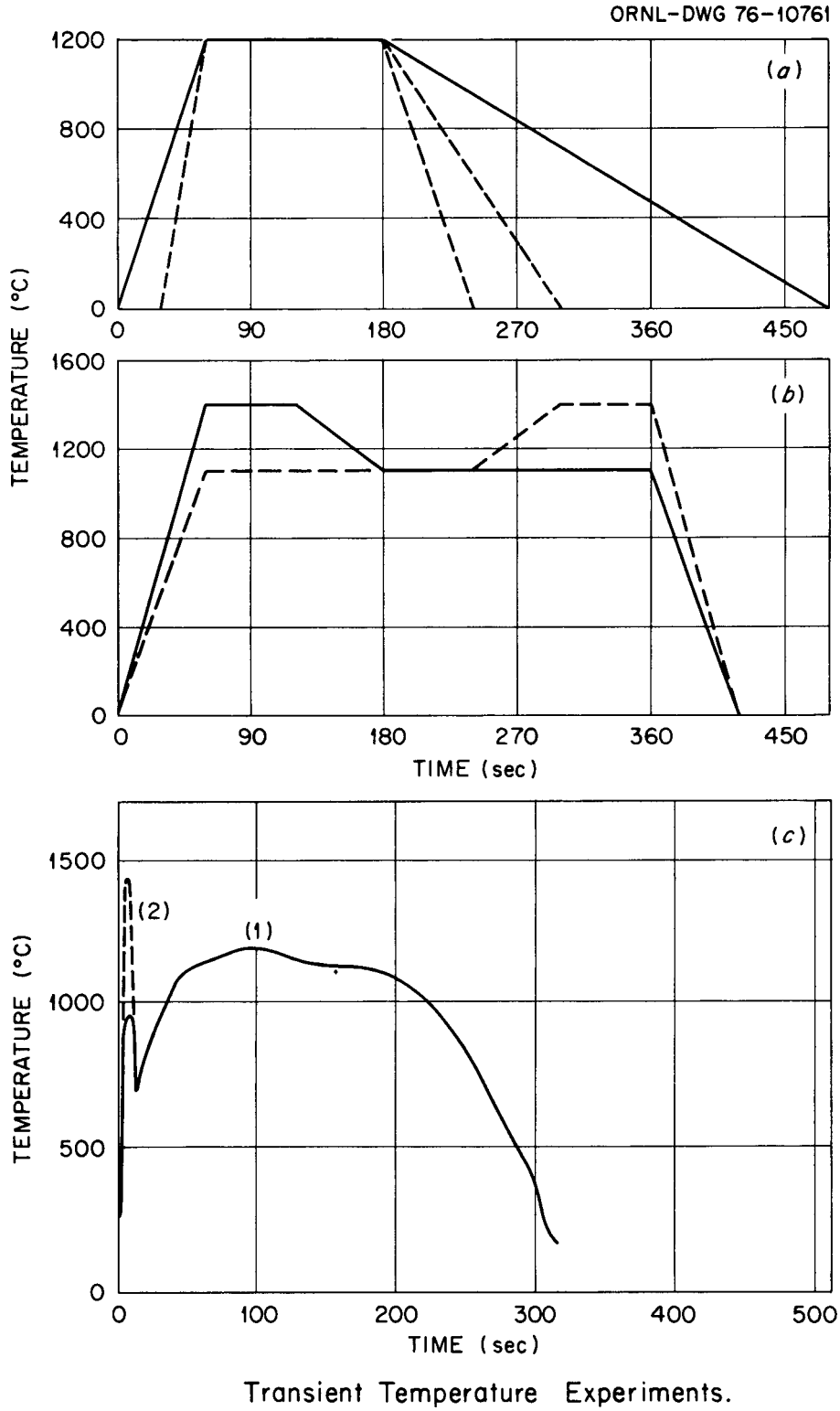

Fig. 12. Schematic representations of the time-temperature profiles of transient temperature oxidation tests.

The results of these tests are currently being analyzed and will be reported fully in the next Quarterly Report. However, we wish to call attention to the oxide and alpha layer thickness measurements (see Table 15) obtained from samples subjected to the transients shown in Fig. 12c.

Table 15. Oxide and Alpha Layer Thicknesses After Hypothetical LOCA Transients

Curve No.	Blow-down Peak Temp. (°C)	(°F)	Layer Thickness oxide μm	alpha μm
1	900	1652	45.8	49.8
2	1400	2552	40.2	52.4

The two experiments were nominally identical except for the maximum temperature reached in the blow-down peak. Thus, assuming ideal oxidation behavior, one expects the second specimen [blow-down peak temperature 1400°C (2552°F)] to exhibit a somewhat thicker oxide layer. As may be seen in Table 15, the reverse was actually the case.

These results are qualitatively similar to data reported by Biederman[5] for a comparable set of experiments, and they indicate that at least certain types of transients may not be treatable in terms of computer codes based on isothermal oxidation data alone. We cannot at this time offer an explanation for this phenomenon, although we have repeated the transients shown in Fig. 12c using specimens made of crystal bar zirconium. The results were comparable to those obtained with Zircaloy-4, and we have, therefore, concluded that the alloying elements in Zircaloy are not responsible for the effect.

Scoping Tests

Mixed Gas Experiments

As a part of the program plan for scoping tests a series of experiments has been performed in which nitrogen, hydrogen, and oxygen have been added to the steam prior to exposing the Zircaloy to it in the MiniZWOK apparatus. These experiments have been completed and are in the process of being analyzed.

Details of the experiments are listed in Table 16. In these tests the specimens were oxidized in the mixed gases at two temperatures with duplicate experiments at each time and temperature listed. These experiments were designed to demonstrate the influence of various gaseous impurities in the steam on the isothermal rate of oxidation of Zircaloy-4. The results of these tests will be presented in the next quarterly report.

Table 16. Steam Impurity Scoping Tests

Temperature (°C)	Temperature (°F)	Oxidation Time (s)		Impurity Concentration (mol %) N_2	O_2	H_2
1100	2012	150	535	10	10	5
1300	2372	25	145	10	10	5

Alloy Composition Variation

In addition to gaseous impurities, small changes in alloy composition have been investigated for possible influence on the isothermal oxidation of Zircaloy in steam. As specified in the original proposal of the ZWOK program, a standard lot of reactor grade Zircaloy-4 tubing* was used for all isothermal and transient temperature oxidation experiments to facilitate comparison with other workers' results. In addition to this standard

*Reactor Grade PWR Zircaloy-4 tubing (Sandvik Special Metals Corp.). Composition (wt %): 1.60 Sn, 0.25 Fe, 0.12 Cr, 0.12 O, 0.009 C, 0.003 N, 0.0025 H.

tubing, additional tubing* has been used to obtain rate constants that will reflect small variations in alloy composition. At temperatures of 1150 and 1500°C (2102—2732°F) rate constant determinations have been made by the procedure documented in previous quarterlies. These experiments are designed to show influences of small variations in alloy content on the oxidation behavior of Zircaloy-4 and will be reported on fully in subsequent reports.

HIGH PRESSURE STEAM OXIDATION

S. H. Jury and J. J. Campbell

We shall perform a series of scoping tests to determine the effect of steam pressure on the isothermal rate of oxidation of Zircaloy-4 in steam. The apparatus to be used for this work is shown schematically in Fig. 13. It consists basically of two interconnected 5 in. diam, stainless steel autoclaves. The lower one, 7 in. long, is a boiler that supplies pressurized steam generated by an internal resistance heater. The desired pressure of saturated steam is attained by controlling the boiler temperature in conjunction with appropriate settings of the pressure control valves.

The upper autoclave, 10 in. long, acts as the reaction chamber. The specimen is a length of PWR Zircaloy-4 tubing, the bottom end of which rests on the specimen support tube attached to the bottom of the boiler. The upper end of the specimen is supported in, but not constrained by, the opening in the instrument head at the top of the autoclave. Steam entering the reaction chamber is confined by a 1 in. diam quartz tube to the annular region between the tube and the specimen. Steam can also flow through the inside of the specimen, or the interior of the specimen can be filled with pressurized argon, which enters through the specimen support tube.

*Reactor grade PWR Zircaloy-4 tubing, "Batch B." Composition (wt %): 1.3 Sn, 0.22 Fe, 0.10 Cr, 0.125 O, 0.010 C, 0.0015 N, 0.0015 H.

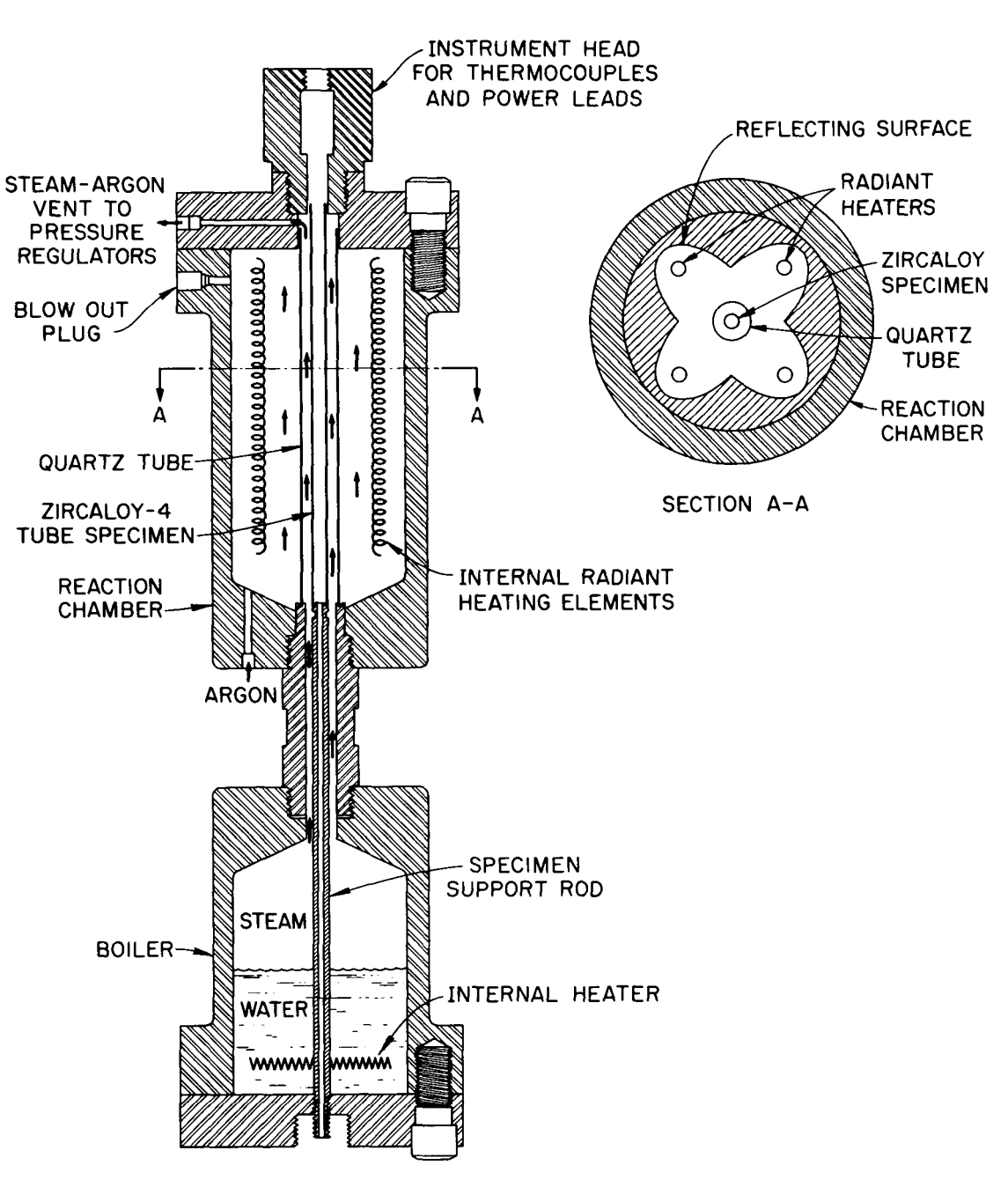

Autoclave for High Pressure Steam Oxidation Studies.

Fig. 13. Schematic drawing of apparatus for high pressure steam oxidation experiments. For the sake of clarity several external ports have been omitted from the drawing.

The specimen is heated to the desired reaction temperature by a specially constructed quad-elliptical radiant heating furnace that is contained within the reaction chamber. The reflector for the furnace is made of stainless steel, and the reflecting surfaces are gold-plated to ensure a high reflectivity. The quartz lamps used in the furnace were undamaged in a hydrostatic pressure test at room temperature and 6.894 MPa (2000 psi).

The reflector for the furnace is cooled by a flow of pressurized argon that enters through a port at the bottom of the reaction chamber. The argon exits through slots (not shown) in the upper closure of the autoclave just above the top of the quartz tube surrounding the specimen. There it mixes freely with steam from the boiler, and both gases then pass out of the system through a pressure regulating valve. Appropriate adjustments of the argon pressure and flow rate should prevent any serious mixing between argon and steam in the vicinity of the specimen.

Suitable ports (not shown) in the instrument head and top closure plate provide access for power leads to the furnace and for two Pt vs Pt—10 wt % Rh thermocouples. One thermocouple will serve as the temperature control couple while the other will be used to measure temperature. Both will be spot welded to the interior of the specimen tube near the center of the furnace.

We believe that this apparatus will allow reasonably accurate tests to be made of the effect of steam pressure on the isothermal rate of oxidation of Zircaloy. The radiant heating furnace is very similar to that used in our MiniZWOK oxidation apparatus. Thus we expect to be able to heat the specimen rapidly to the reaction temperature and to control temperature accurately. The fast response of the furnace and the cooling effects of the steam should prevent significant specimen self-heating during oxidation. The constant flow of steam through the autoclave should make hydrogen blanketing impossible. Temperature measurement problems may be more severe than in the MiniZWOK apparatus, but it should be possible to minimize such difficulties by making oxidation rate measurements in the autoclave at both atmospheric and higher pressures, thus establishing an "internal standard" for comparison to the high temperature results.

The high pressure apparatus is currently being assembled, and we hope to begin testing during July. Tests will be performed at 900 and 1100°C (1652–2012°F) at a maximum steam pressure of 3.45 MPa (500 psi).

DIFFUSION OF OXYGEN IN β-ZIRCALOY-4

R. A. Perkins

The study of the diffusivity of oxygen in β-Zircaloy-4 has been completed. The abstract of the final report, which will be issued early in July 1976 as ORNL/NUREG-19, is given below.

At the end of a hypothetical loss-of-coolant-accident in a Light Water Reactor the mechanical properties of the "prior" beta region of the Zircaloy fuel clad will be determined to a large extent by its oxygen content. For this reason the diffusion of oxygen-18 in β-Zircaloy-4 has been measured from 900 to 1500°C (1652–2732°F), and survey measurements have been made for β-zirconium and β-Zircaloy-2. The tracer diffusivity was measured over the entire temperature range and the chemical diffusivity from 1100 to 1500°C (2012–2732°F). The experiments were performed by using oxygen-18 as the tracer and activating it by proton bombardment. Some complementary measurements were made using Auger Electron Spectroscopy. The results indicated that the tracer and chemical diffusivity of oxygen in β-Zircaloy-4 are statistically identical, and there is no oxygen concentration dependence over the oxygen concentration range studied, 0.1 to 0.6 wt %. The temperature dependence of the diffusivity from 1000 to 1500°C (1832–2732°F) is

$$D = 2.48 \times 10^{-2} \exp(-28200/RT) \text{ cm}^2/\text{s} .$$

Below 1000°C (1832°F) the diffusivity dropped sharply because a two phase α + β mixture was present. The results for the β-Zircaloy-2 and β-zirconium indicated that the alloying additions have no influence upon the oxygen diffusivity. The combination of three sets of boundary conditions (thin film tracer diffusion, single-phase chemical diffusion couple and phase-boundary-movement chemical diffusion couple) and two methods of oxygen profiling (oxygen-18 radioactivation and Auger Electron Spectroscopy) were used to increase the confidence in the results. The current results are about 50% lower than the previous results of Mallett, Albrecht, and Wilson. The diffusivity of oxygen-16 is expected to be 6% greater than that for oxygen-18.

DIFFUSION OF OXYGEN IN OXYGEN-STABILIZED ALPHA-ZIRCALOY-4

R. A. Perkins

Using the techniques which were developed to measure the diffusivity of oxygen in β-Zircaloy-4, the tracer diffusivity of oxygen in the α phase was determined at 1050, 1200, and 1350°C (1922, 2192, and 2462°F) for oxygen concentrations of 2.4, 2.5, and 3.1 wt %, respectively. The specimens were enhanced in oxygen by repeated oxidation at 800°C (1472°F) in flowing oxygen and homogenization at 1500°C (2732°F) in vacuum. The results for the tracer diffusion measurements are shown in Fig. 14.

The diffusivity data of Mallett et al.[6] and Chung et al.[7], shown in Fig. 14, were obtained by phase boundary movement techniques which assume that the oxygen diffusivity is independent of oxygen concentration and measure the chemical diffusion coefficient. Therefore, to compare the present results to the previous data, the tracer diffusivity must be related to the chemical diffusivity. This relationship is[8]

$$D_O = D_O^* \left(1 + \partial \ \ell n \ \gamma_O / \partial \ \ell n \ N_O\right) \qquad (8)$$

where

D_O is the chemical diffusivity of oxygen,

D_O^* is the tracer diffusivity,

γ_O is the activity coefficient of oxygen in α-Zircaloy-4, and

N_O is the atom fraction of oxygen in solution in the α-Zircaloy-4.

The quantity in parenthesis in Eq. (8) can be evaluated using the thermodynamic data for the solution of oxygen in α-Zircaloy-4. The thermodynamic data for oxygen in α-zirconium are available[9] and were used to make the adjustment.

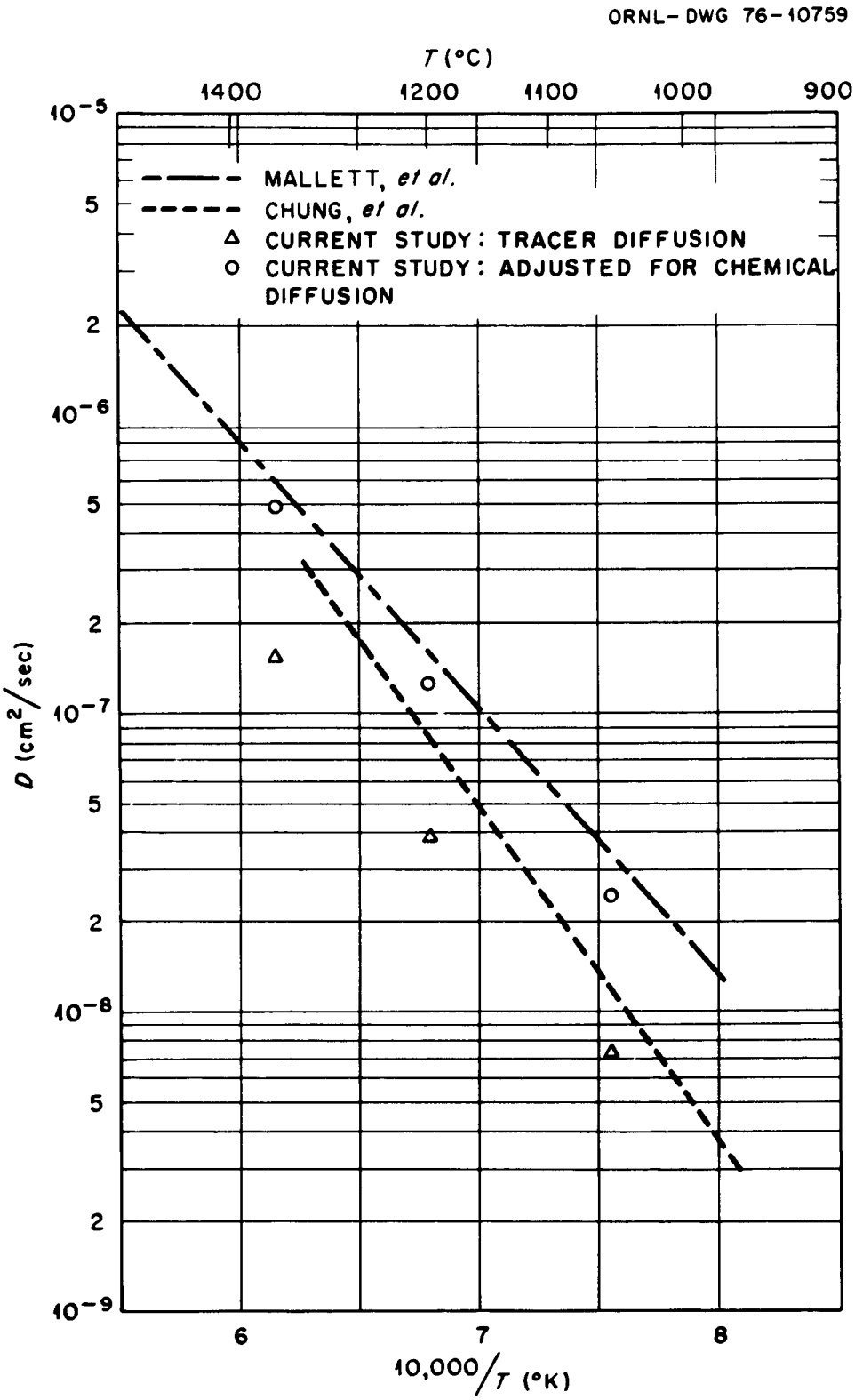

Fig. 14. Arrhenius plot of the oxygen diffusivity in α-Zircaloy.

The activity coefficient of oxygen in α-zirconium can be related to the oxygen pressure over the metal by[10]

$$\gamma_O = P_{O_2}^{1/2} / K_O N_O \ , \tag{9}$$

where P_{O_2} is the oxygen pressure over the metal when N_O oxygen is dissolved in the metal and

$$K_O \equiv \exp[(\mu_O^* - \tfrac{1}{2}\mu_{O_2}^o)/RT] \ , \tag{10}$$

where

μ_O^o is the chemical potential of oxygen in the gas in its standard state and

μ_O^* is the chemical potential of oxygen in the metal in a hypothetical standard state corresponding to extrapolation from infinite dilution along the Henry Law gradient.

The convention which is used is that as N_O goes to zero, γ_O goes to one. From Eq. (9) one obtains

$$\partial \ln \gamma_O / \partial \ln N_O = \partial \ln P_{O_2}^{1/2} / \partial \ln N_O - 1 \ .$$

Figure 15 shows a plot of $\ln P_{O_2}^{1/2}$ versus $\ln N_O$ at 1400 and 1600°K (2061—2421°F) and demonstrates that, despite the large solubility of oxygen in α-zirconium, $\partial \ln \gamma_O / \partial \ln N_O$ does not vary with oxygen concentration for $\ln N_O > -3.9$ (∿2 at. %). Values for $\partial \ln \gamma_O / \partial \ln N_O$ of 2.33 at 1400°K (2061°F) and 2.18 at 1600°K (2421°F) were obtained from the curves and used in Eq. (8) to convert the measured tracer diffusivities to chemical diffusion coefficient values.

Although γ_O is invariant with respect to oxygen concentration over the range of interest in this study (2 to ∿30 at. %), D_O is by no means independent of oxygen concentration. At infinite dilution γ_O is by definition unity. Thus $\partial \ln \gamma_O / \partial \ln N_O$ must vary from zero to ∿2 for $0 < N_O < \sim 0.02$ before becoming constant. The oxygen concentration at the upper end of the region of variation of D_O is uncertain, but a value of ∿ 2 at. % ($\ln N_O \approx -4$) is indicated by the fact that the

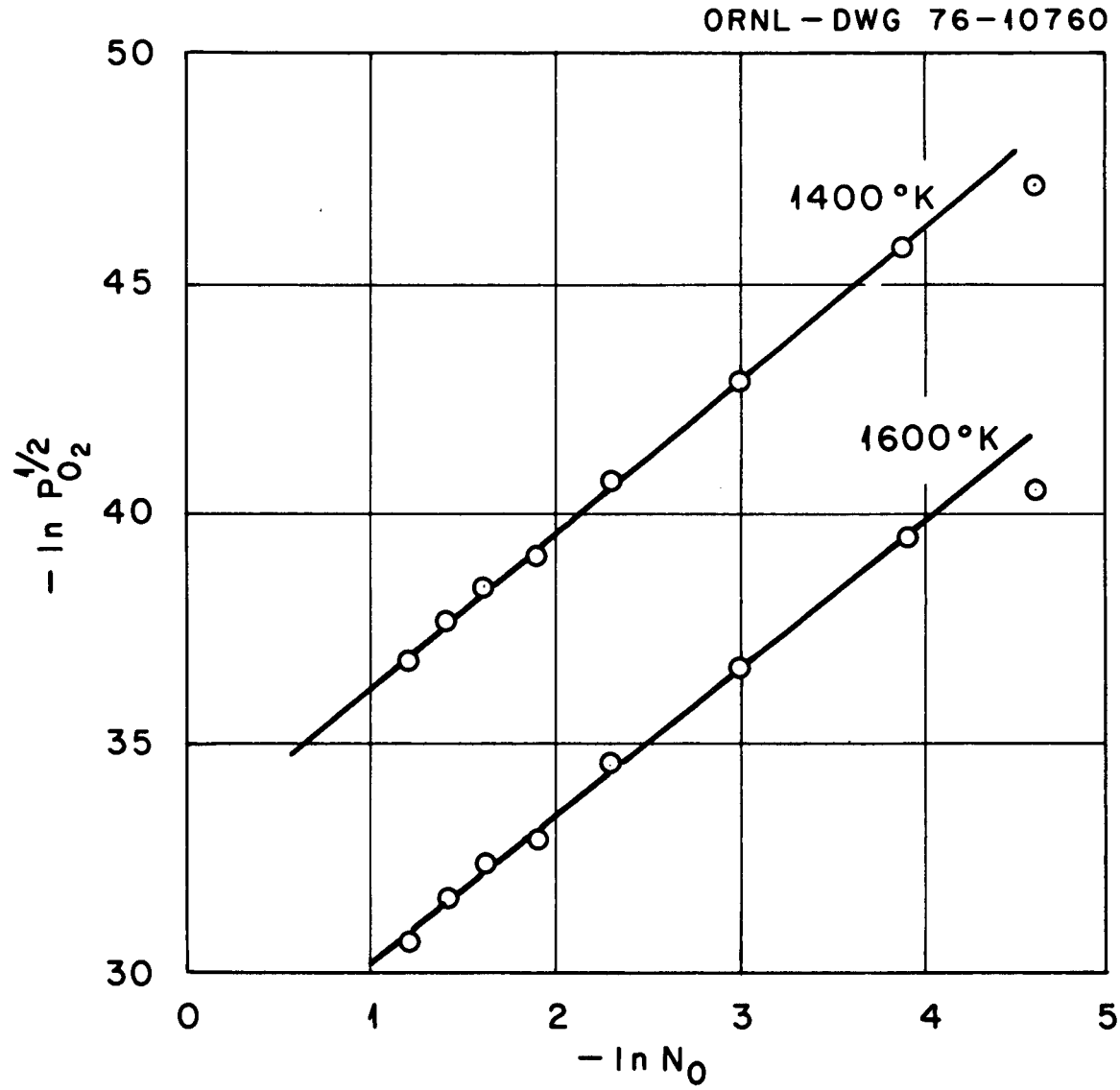

Fig. 15. Logarithm of the equilibrium solubility of oxygen in α-zirconium versus the logarithm of the oxygen pressure over the metal.

last data point at the right of the curves in Fig. 15 in both instances lies below the curves themselves, suggesting that a decrease in $\partial \ln \gamma_O / \partial \ln N_O$ has already started.

As indicated in Fig. 14 differences exist between the alpha diffusivity values determined by Mallett and by Chung. Since only three diffusivity values were obtained in the current study, our results do not furnish an adequate basis for choosing between the older data sets. In fact, the purpose of these scoping tests was to investigate the nature of the dependence of D_O on oxygen concentration and thus to assess the validity of the assumption, inherent in the work both Mallett and Chung, that D_O is independent of oxygen concentration. Our study shows that D_O is invariant over the range of oxygen concentrations of real interest and that chemical diffusivity values previously obtained should in principle be suitable for use in computer code predictions of the oxidation behavior of Zircaloy.

REFERENCES

1. J. V. Cathcart, et al., *Zirconium Metal–Water Oxidation Kinetics I. Thermometry*, ORNL-5102, (February 1976).

2. J. V. Cathcart, *Quarterly Progress Report on the Zirconium Metal–Water Oxidation Kinetics Program Sponsored by the NRC Division of Reactor Safety Research for October–December 1975*, ORNL/TM-5248 (March 1976).

3. J. V. Cathcart, *Quarterly Progress Report on the Zirconium Metal–Water Oxidation Kinetics Program Sponsored by the NRC Division of Reactor Safety Research for January–March 1976*, ORNL/NUREG/TM-17, (May 1976).

4. J. V. Cathcart, *Quarterly Progress Report on Reactor Safety Programs Sponsored by the NRC Division of Reactor Safety Research for October–December 1974 I. Light Water Reactor Safety*, ORNL/TM-4805, (April 1975), Chapt. 4.

5. R. R. Biederman and W. G. Dobson, "A Study of Zircaloy-Steam Oxidation Reaction Kinetics," *Fifth Interim Progress Report, January 16, 1976 through April 15, 1976, Project No. 249-1*, Electric Power Research Institute, Palo Alto, Calif.

6. M. W. Mallett, W. M. Albrecht, and P. R. Wilson, "The Diffusion of Oxygen in Alpha and Beta Zircaloy 2 and Zircaloy 3 at High Temperatures," *J. Electrochem. Soc.* 106, 181–84 (1959).

7. H. M. Chung, A. M. Garde, and T. F. Kassner, *Light Water Reactor Safety Research Program: Quarterly Progress Report, July–September 1975, Chapt. III*, ANL-75-72.

8. L. S. Darken, "Diffusion, Mobility and Their Interaction through Free Energy in Binary Metallic Systems," *Trans. AIME*, 175, 184–201 (1948).

9. K. L. Komarek and M. Silver, "Thermodynamic Properties of Zirconium-Oxygen Alloys," *Proc. of Symposium on Thermo of Nuclear Materials* by IAEA, Vienna, 749–74 (1962).

10. K. Denbigh, *The Principles of Chemical Equilibrium*, Second Edition, Cambridge University Press, Cambridge, Great Britian, 270–73 (1966).

ORNL/NUREG/TM-41
NRC-3

Internal Distribution

1. C. K. Bayne
2. M. Bender
3. C. J. Borkowski
4. J. R. Buchanan
5. J. J. Campbell
6. K. R. Carr
7-32. J. V. Cathcart
33. R. H. Chapman
34. W. B. Cottrell
35. F. L. Culler
36. D. G. Davis
37. R. E. Druschel
38. G. G. Fee
39. D. E. Ferguson
40. J. H. Freels
41. J. A. Hawk
42. R. A. Hedrick
43. M. R. Hill
44. D. O. Hobson
45. S. H. Jury
46. T. G. Kollie
47. B. C. Leslie
48. T. S. Lundy
49. F. C. Maienschein
50. D. L. McElroy
51. C. J. McHargue
52. R. A. McKee
53. C. S. Meadors
54. F. H. Neill
55. R. E. Pawel
56. R. A. Perkins
57. H. Postma
58. E. T. Rose
59. R. L. Shipp
60. D. B. Trauger
61. J. R. Weir
62. R. K. Williams
63. Patent Office
64-65. Central Research Library
66. Document Reference Section
67-71. Laboratory Records Department
72. Laboratory Records (RC)

External Distribution

73-80. Director, Division of Reactor Safety Research, Nuclear Regulatory Commission, Washington, D.C. 20545
81. Director, Reactor Division, ERDA, ORO
82. Director, Research and Technical Support Division, ERDA, ORO
83-402. Given distribution as shown in NRC categories 1, 3 (25 copies — NTIS)